18th Australasian Wind Engineering Society Workshop
McLaren Vale, South Australia
6-8 July 2016

An experimental investigation of wind loads on a 3:1 rectangular cylinder during ramp-up flows: effects of blockage ratio

[1]T. Yang, [1]M.S. Mason

[1]School of Civil Engineering, University of Queensland, St Lucia, Qld, Australia

Abstract

Wind pressures were measured on two 3:1 ratio rectangular cylinders during ramp-up (unsteady) and steady flow conditions using an actively controlled wind tunnel. For unsteady tests, the tunnel was programmed to accelerate (ramp) from zero to a target wind speed over a short-time duration. Both steady and unsteady loads were measured and analysed for the two cylinders, which exhibited blockages ratios of 7.9% and 2.6%. Results for both models displayed similar characteristics, but the smaller model had marginally larger peak pressure coefficients in the periodic reattachment region on the top and bottom faces during both steady and unsteady tests. The smaller model also exhibited a more rapid increase in time-varying mean drag and peak lift coefficients during the unsteady ramp-up tests when compared with the larger model results.

Introduction

The aerodynamics of rectangular cylinders has long been of interest to the wind engineering community. Many civil structures exhibit such a cross sectional shape, e.g. high-rise buildings, bridge decks, therefore, understanding the wind loads applies to these bodies has significant practical benefit. Given this, wind effects on rectangular cylinders has been extensively studied. Laneville and Williams (1979) investigated the effect of intensity and large scale turbulence on the drag coefficient of 2D rectangular cylinders. They showed that it was turbulence intensity, rather than scale, that had the greater influence on the aerodynamics of cylinders. Nakamura and Ohya (1984) studied the effects of turbulence on the mean flow past rectangular cylinders and found that small-scale turbulence increased the growth rate of shear layers while large-scale turbulence weakens regular vortex shedding. Li and Melbourne (1999) presented the effects of free-stream turbulence on surface pressure fluctuations on 2D rectangular cylinders, with a particular focus on the nature of separation and reattachment in turbulent flows. Larose and D'Auteuil (2008) selected rectangular prisms with aspect ratio 2, 3 and 4 to 1 (afterbody:front face) and studied the surface pressures as well as lift, drag and pitching moment for a range of turbulence regimes and Reynolds Numbers (Re). They concluded that with an increase in Re, a gradual increase in drag coefficient was observed, while lift coefficients were more or less invariant.

The present study aims to investigate the influence of model size on measured surface pressure and resulting drag and lift force coefficients for aspect ratio 3:1 rectangular cylinders in steady and unsteady flow conditions. Two model sizes are investigated, one with a blockage ratio of 7.9% and the second 2.6%. Differences in mean and peak pressure and force coefficients will be highlighted and discussed.

Experimental setup and procedure

Wind tunnel tests were conducted in an Eiffel-type open circuit wind tunnel with cross sectional dimensions of 0.76m × 0.76m. Flow is driven by a single vane-axial fan located downstream of the test section, which can be programmed to accelerate flow from zero to a target wind speed, U_t, over a short time period. For steady flow experiments the mean tunnel wind speed was set to U_t = 25.6 m/s with an associated turbulence intensity of less than 1%. Unsteady flow experiments focused on a single ramp-up style event that accelerated from an initial still condition (i.e. U = 0 m/s) to U_t over approximately 2.5 seconds. Figure 1 shows the ramp time history measured at the reference position indicated in Figure 2 for 30 repeat runs. The test to test repeatability of the flow acceleration process is clearly evident.

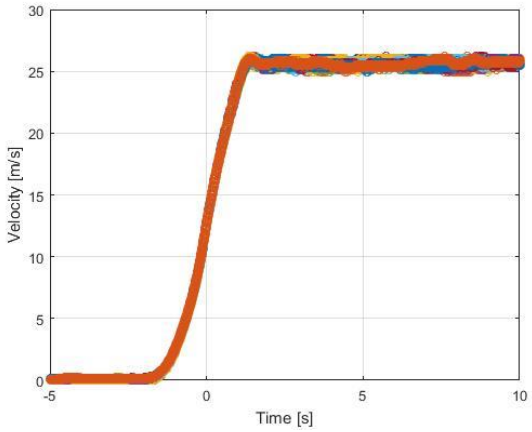

Figure 1. Unsteady flow ramp-up time history for 30 test runs overlaid. Time = 0s corresponds to the point in time where the reference velocity is equal to $U_t/2$.

Two rectangular cylinders were tested in this study. The first had cross sectional dimensions of $B \times D$ equal to 180mm × 60mm (Big model; 7.9% tunnel blockage) and the second, 60mm × 20mm (Small model; 2.6% tunnel blockage). Figure 2 shows both models mounted in the upwind section of the University of Queensland wind tunnel. Each was fixed horizontally and equipped with circular end plates a distance of 300mm from the model centre line to promote two-dimensionality of the flow. Test Reynolds Numbers for the two setups were 1.0×10^5 and 0.33×10^5 for the big and small models, respectively, based on windward face dimension and U_t.

Surfaces pressures around the centreline of both rectangular cylinders were measured during the experiment. The big model had 28 taps on the top and bottom faces and 12 pressure taps on the windward and leeward faces. The small model had 12 taps on the top and bottom faces and 3 taps on the windward and leeward edges. All pressure taps were connected to a Scanivalve ZOC-33 pressure scanning system through 1.5m length, 1.5mm internal diameter PVC tubing. Distorted pressure signals received by the transducer in both amplitude and phase were corrected according to the theoretical frequency response functions of Bergh and Tijdeman (1965).

For the purpose of generating normalised pressure coefficients, reference velocities for steady and unsteady tests were recorded using a single-wire hotwire 100mm from the top of the wind tunnel, as shown in Figure 2. The hotwire was aligned with the front face of each model. Static wind tunnel pressures were also measured at a pressure tap located on the floor of the wind tunnel in this same plane. Both pressure and velocity measurements were sampled at 600 Hz, with steady flow tests run for 180 seconds.

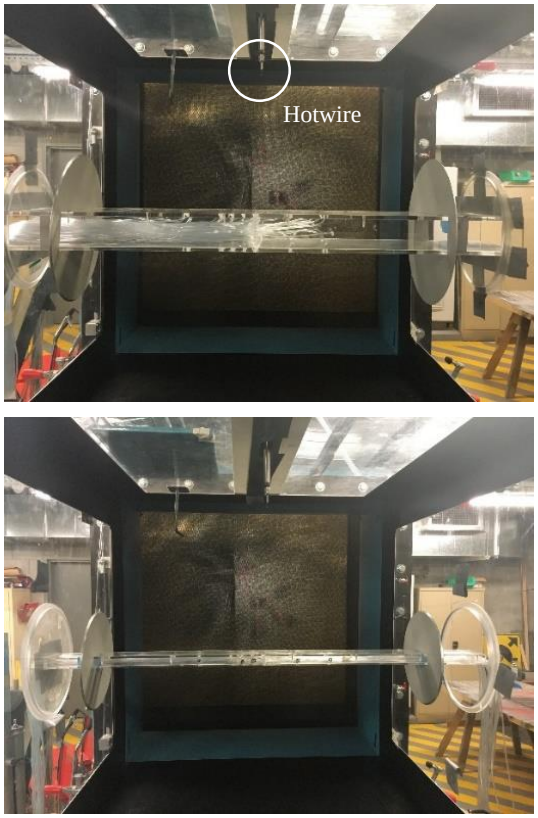

Figure 2. Experimental setup: big rectangular cylinder with 180×60mm cross section (top) and small one with 60×20mm cross section (bottom).

Results and discussions

Steady flow

Mean, standard deviation and peak pressure coefficients for each tap around the surfaces of both models were calculated using Equation (1). p_t is the mean, standard deviation and peak pressure measured at each individual tap, p_s is the mean static pressure measured at the reference tap located on the tunnel floor, ρ is the density of air and U_t is the mean velocity measured by the hotwire at the reference location. Peak values are defined as the 95th percentile value on an empirical CDF of the sampled pressure data.

$$C_{p,s} = \frac{p_t - p_s}{{}^1/_2 \rho {U_t}^2} \quad (1)$$

Figure 3 shows mean, standard deviation and peak $C_{p,s}$ distributions around the centreline of both models. As expected, the windward face of both models shows positive pressure maxima of approximately 1 near their centre, and decreasing values towards the edges. Almost uniform mean $C_{p,s}$ of -1.0 are evident along the windward half of both top and bottom faces, with standard deviation and peak $C_{p,s}$ values of around 0.1 and -1.2. For the leeward half of these faces, mean $C_{p,s}$ gradually drops to -0.3 near to the leeward end, while the standard deviation increases until around 0.8B from the leading edge before slightly decreasing before the leeward edge of the model. Peak pressure coefficients reach a maximum at around 0.65B from the leading edge. The mean $C_{p,s}$ on the leeward face is almost uniform, at -0.5, and both the standard deviation and peak $C_{p,s}$ reach a minima at the middle points of this face.

Both big and small models follow the same overall pressure distribution pattern. Figure 3 (c) shows the pressure coefficient ratios ($C_{p,s}$ - small / $C_{p,s}$ - big) that allows a simple comparison of results between the two models. For windward and leeward surfaces, the ratios of mean and peak coefficient varies between 0.9 and 1.1, with the value at mid-height tending to be the minimum. For top and bottom surfaces, the ratios of peak and mean are predominantly around 1.0, while in the region near the trailing edge the mean value goes up to 1.2~1.3. The peak ratio, however, reduces below 1.0.

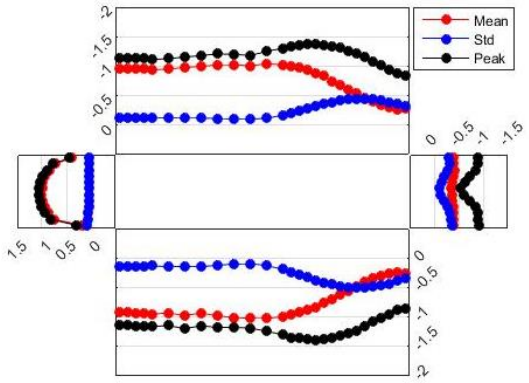

(a) Big model

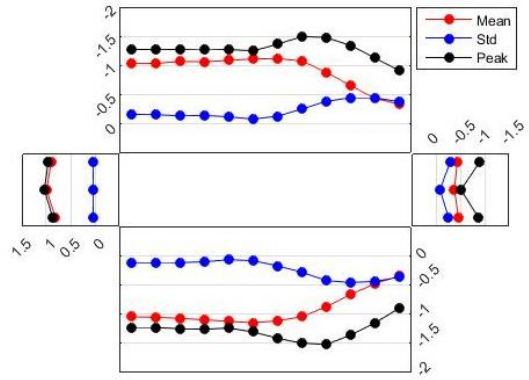

(b) Small model

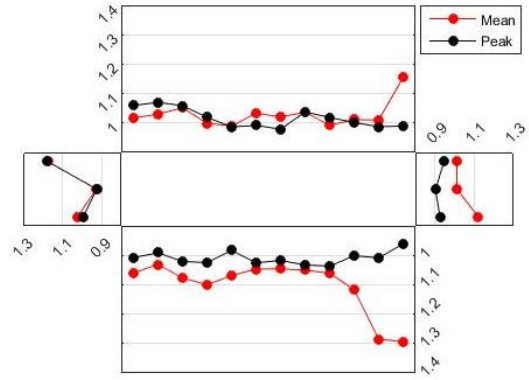

(c) Coefficient ratios

Figure 3. Mean, standard deviation and peak pressure coefficient distribution around model centreline. (a) big model, (b) small model, (c) Coefficient ratio (small/big).

Unsteady flow

To investigate how pressure distributions around both cylinders change over the ramp-up period, each of the 30 tests were aligned in time and the ensemble tap or integrated force data were analysed. Within each test, velocity and pressure data were aligned by assigning t = 0s to the first exceedance of $U_t/2$ in the reference hotwire velocity record and to the first exceedance of $(p_t - p_s)/4$ in the pressure time history of the top face tap 0.65B from the leading edge. This location corresponds to the maximum peak pressure occurring on the top and bottom surface in steady flow

(Figure 3). Unsteady pressure, drag and lift coefficients were calculated using Equations (2-4).

$$C_{p,t} = \frac{p_t(t) - p_s(\tilde{t})}{1/2 \rho U(\tilde{t})^2} \quad (2)$$

$$C_{D,t} = \frac{\sum[(p_t(t) - p_s(\tilde{t}))\delta d]}{1/2 \rho U(\tilde{t})^2 D} \quad (3)$$

$$C_{L,t} = \frac{\sum[(p_t(t) - p_s(\tilde{t}))\delta d]}{1/2 \rho U(\tilde{t})^2 B} \quad (4)$$

For all normalisations, a time-varying reference velocity, $U(\tilde{t})$, is used. The tilde above t on both the static pressure and velocity signifies that a moving average filtered (0.1s) time history is used. In addition, pressures are integrated around the surface of each model to transform them into drag, $C_{D,t}$, and lift coefficients, $C_{L,t}$. The summation in Equations (3-4) are of the individual differential tap pressures multiplied by the tributary side length (δd) for each tap. D and B represent the depth and width of model, respectively.

Figure 4 shows the ensemble unsteady pressure coefficient, $C_{p,t}$, normalized by transient reference wind speeds, for the tap 0.65B from the leading edge of the top surface for all 30 tests. Large scatter is seen for t < -1.5s for both models, which coincides with the beginning of the ramp where very small reference velocities are present. This region is therefore of little consequence when considering wind loads on a structure. As the ramp continues, scatter tightens near t = -0.5s before expanding around a gradually increasing mean suction pressure throughout the ramp. The mean and peak pressure coefficients fully stabilize at approximately t = 1.0s for the small model and t = 0.5s for the big model, which is shortly after the flow ceases ramping. Both models display similar characteristics throughout the ramp, except that the small model exhibits larger peak suction pressure coefficients until stabilizing at 1.0s.

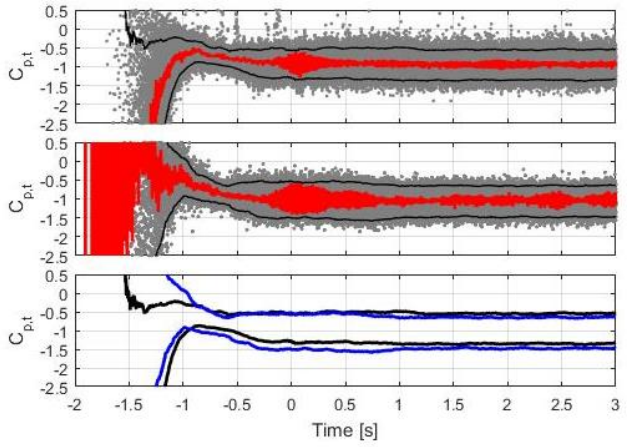

Figure.4. Unsteady pressure coefficient time histories, $C_{p,t}$, for the top face tap 0.65B from the leading edge. Grey dots show sample points for each of the 30 tests. The solid red line shows the ensemble average of these data and the two black lines show the 5% and 95% percentile bounds (i.e. peaks). Top figure shows the $C_{p,t}$ time-histories for the big model; middle figure indicates the $C_{p,t}$ time-histories for the small model; Bottom figure indicates the peak bounds of big model (black lines) and small model (blue lines).

Collating peak $C_{p,t}$ data for all pressure taps around both models, the pressure coefficient distribution at six time steps throughout the ramp-up process is plot in Figure 5. At t = 1.5s, the peak pressure coefficient distribution is almost identical to that shown in Figure 3, indicating the flow regime is approaching steady flow conditions. For t < 0 s, the top, bottom and lee faces exhibit peak $C_{p,t}$ distributions evolving from what appears to be attached flow to the final steady flow pattern. This suggests the flow physics are changed during the ramp-up process. Both models display similar evolutionary processes, and it is hypothesised that the expanding profiles exist because the vortex shedding process is developing throughout the ramp.

Figure 5 (c) displays the ratio of pressure coefficients for the two models at the six time steps shown in (a) and (b). For the windward and leeward surfaces, the ratio evolution is similar with a decreasing trend throughout the ramp-up process. A similar trend is observed on the top and bottom faces, but unlike the windward and leeward faces where the final ratio is below 1.0, the ratio on these faces remains above unity.

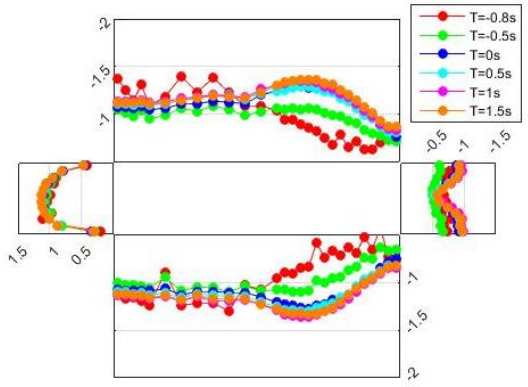

(a) Big model

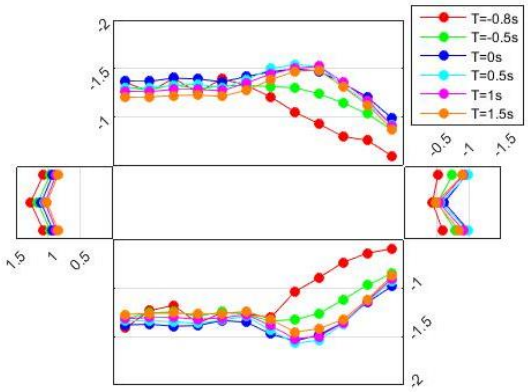

(b) Small model

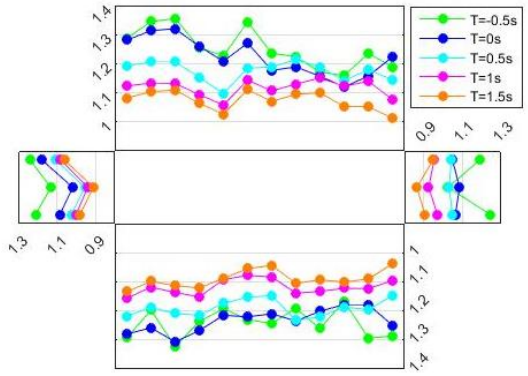

(c) Coefficient ratios

Figure 5. Time dependent ensemble peak pressure coefficient distributions around the two models at multiple times during the ramp-up process.

Integrating surface pressures around each model, unsteady drag and lift coefficients normalized by transient reference wind speed are calculated using Equation (3) and (4) (Figure 6 & 7). Noting that the ramp begins at approximately t = -1.5s, and as noted for Figure 4, a rapid tightening of peak bounds in both drag and lift coefficient is seen at t = -0.7s for both models. In a mean sense the

lift coefficient remains constant throughout the ramping process however the amplitude of its fluctuation appears to undergo a slow increase throughout this period. This amplitude rapidly increases over the period -0.5s < t < 0s, but still appears to increase until ramping ends at around 1.0s. This process is less pronounced for the small model, and peaks remain relatively constant following the initial amplitude increase. Drag coefficient, on the other hand, displays a steady increase in the mean value throughout the ramp. The mean drag coefficient for the big model steadily increases from 1.1 to 1.3, while for small model, it increases from 1.0 to 1.5 then back to 1.3. There does, therefore, appear to be some minor differences between the two model results when considering raw magnitudes, but both appear to undergo the same physical processes throughout the ramping phase.

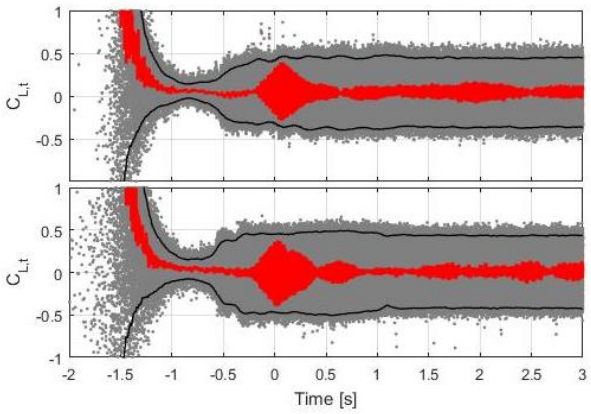

Figure 6. Ensemble unsteady lift coefficients time histories during ramp-up process for big model (top) and small model (bottom).

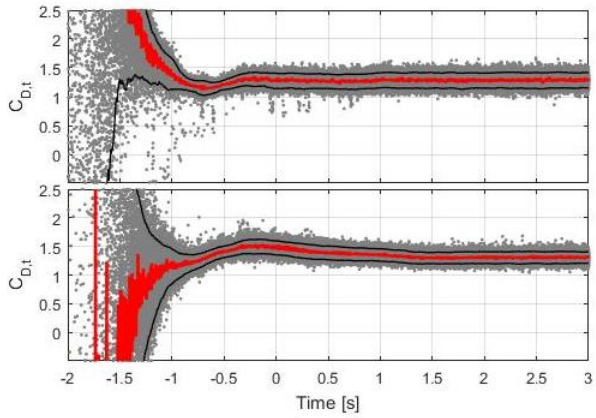

Figure 7. Ensemble unsteady drag coefficients time histories during ramp-up process for big model (top) and small model (bottom).

Figure 8 shows the peak bounds of unsteady $C_{D,t}$ and $C_{L,t}$ time-histories for both models, allowing for a more direct comparison between these data. The small model appears to display a small overshoot (Takeuchi et al. 2008) in both the mean drag and peak lift coefficients, which are not present for the big model. This difference is still the focus of continued investigation and will be reported on further in future work.

Conclusions

Wind pressures on two rectangular cylinders with the same aspect ratio (3:1), but different sizes (and therefore blockage ratios), were measured in steady and unsteady ramp-up flow conditions. Results show that both big and small models exhibit almost identical pressure distribution patterns when measured in steady flow. The only area of minor difference was found to be on the lee half of the top and bottom faces where the flow appears to be periodically reattaching to the model. For the unsteady ramp-up tests, the pressure distribution on top, bottom and lee faces of both models evolves throughout the ramping period from what appears to be an initially attached flow to that of periodic shedding, as displayed in steady flow. This shows that the flow physics are continually changing as the incident flow accelerates. Similar results were found for both bodies, but the small model displayed marginally higher peak drag and lift coefficients.

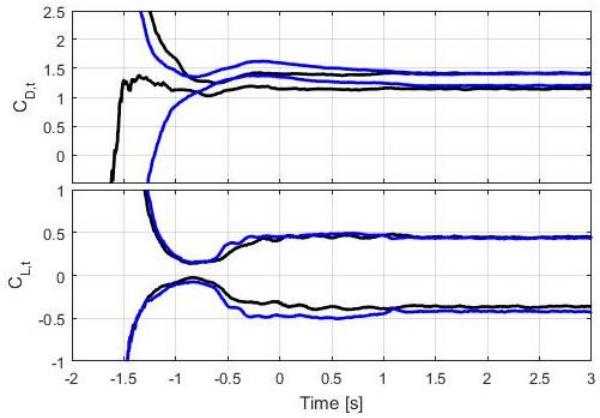

Figure 8. Ensemble peak bounds of unsteady drag and lift coefficients time histories during ramp-up process for the big model (black lines) and small model (blue lines).

Acknowledgements

The authors would like to acknowledge funding for this project made available through University of Queensland Grant NS-1501.

References

Bergh, H. and H. Tijdeman (1965). Theoretical and experimental results for the dynamic response of pressure measuring systems. Nationaal Lucht-en Ruimtevaartlaboratorium.

Laneville, A. and C. D. Williams (1979). "The effect of intensity and large scale turbulence on the mean pressure and drag coefficients of 2D rectangular cylinders." Proc. 5th Int. Conference on Wind Effects on Building and Structures, Fort Collins, Colorado.

Larose, G. L. and A. D'Auteuil (2008). "Experiments on 2D rectangular prisms at high Reynolds numbers in a pressurised wind tunnel." *Journal of Wind Engineering and Industrial Aerodynamics* 96.6: 923-933.

Li, Q. S. and W. H. Melbourne (1999). "Turbulence effects on surface pressures of rectangular cylinders." *Wind and Structures* 2.4: 253-266.

Nakamura, Y. and Y. Ohya (1984). "The effects of turbulence on the mean flow past two-dimensional rectangular cylinders." Journal of Fluid Mechanics149: 255-273.

Saathoff, P. J. and W. H. Melbourne (1989). "The generation of peak pressures in separated/reattaching flows." *Journal of Wind Engineering and Industrial Aerodynamics* 32.1: 121-134.

Takeuchi, T., Maeda, J. and Hiromasa Kawashita (2008). "The overshoot of aerodynamic forces on a railcar-like body under step-function-like gusty winds." Sixth International Colloquium on Bluff Body Aerodynamics & Applications, Milano, July.